Submitted to ADVANCED ENERGY MATERIALS

DOI: 10.1002/ (aenm.201400614)

Enhanced Light Harvesting in Semitransparent Organic Solar Cells using an Optical Metal Cavity configuration

By *Francesco Pastorelli*, *Pablo Romero Gomez*, *Rafael Betancur*, *Alberto Martinez-Otero, Paola Mantilla-Perez, Nicolas Bonod* and *Jordi Martorell**

[*] Prof. J. Martorell, F. Pastorelli, P. R. Gomez, R. Betancur, A. Martinez-Otero
ICFO–Institut de Ciencies Fotoniques, 08860 Castelldefels (Barcelona), Spain

E-mail: jordi.martorell@icfo.eu

J. Martorell
Departament de Física i Enginyeria Nuclear, Universitat Politècnica de Catalunya, 08222 Terrassa, (Spain)

F. Pastorelli, N. Bonod
CNRS, Aix Marseille Université, Centrale Marseille, Institut Fresnel, UMR 7249,
13013 Marseille, France

Keywords: Photovoltaics, solar cells, transparent, organics, optical trapping

Recent developments in the field of organic photovoltaics have demonstrated the enormous potential of such technology for integration into renewable energy generation elements that require a certain degree of transparency. It has been experimentally shown that 30% transparent polymer solar cells may exhibit power conversion efficiencies above 5% in single junction devices[1] and above 7 % for tandem ones[2]. Typically, in an organic cell the active material layer is sufficiently thin to present visible transparencies higher than 50%. However, semi-transparency in organic cells can only be achieved when the opaque back metal contact is replaced by a semi-transparent thin electrode[1-18]. The use of two, front and back, semi-transparent electrodes automatically leads to a decrease in the effectiveness of the light harvesting capacity of the solar cell[1,4-23]. Several approaches have been considered to partially recover such lost light harvesting effectiveness at those wavelengths invisible to the eye. Recently, using a non-periodic one-dimensional photonic crystal the short circuit current (J_{sc}) of a semi-transparent cell was brought close to 80% the one from the corresponding opaque cell. The multilayer dielectric structure (MLD) was designed ad hoc to enhance the external quantum efficiency at the near IR and UV wavelengths while maintaining transparency in the visible[1]. The combined use of an anti-reflection coating (ARC) on the front of the cell and a Bragg reflector on the back was also implemented to reach semi-transparent cells performing at 71% of the corresponding opaque one[18].

In the current study we propose to enclose the active material layer in between two metal electrodes that constitute the essential elements of an optical cavity designed to optimize photon trapping inside the cell. At the same time such electrodes are kept sufficiently thin to ensure a visible transparency higher than 20%. The visible transparency of a semi-transparent device corresponds to the integral of the transmission weighted by the product of the human

eye photopic spectral response with illumination from the white standard illuminant CIE-D65.[1] To increase light trapping, while maintaining a sufficient transparency in the visible, an ARC is deposited on top of the front metal contact while a non-periodic MLD is inserted in between the back metal contact and the substrate. As noted below the optimal layer configuration for such MLD was designed specifically for the cell architecture used. With a device architecture as the one shown schematically in **Figure 1**, we achieved semi-transparent cells whose PCE was 5.3%, corresponding to 90% the PCE of the opaque cell. The visible transparency of such cells differed little from the semi-transparent cell which did not include the MLD, while the external quantum efficiency (EQE) closely matched that of the opaque cell

We fabricated two different types of semi-transparent cells (STC1 & STC2) and an opaque cell, which we used as the reference cell to evaluate the PV performance of the semi-transparent cells. The opaque cell was in an inverted configuration with the following architecture: As active material we used a thin layer of PTB7:$PC_{71}BM$ blend, which using an atomic force microscope (AFM) in semicontact mode we measured to be 90 nm thick, very close to the 100 nm used in all the optical simulations. The bottom electrode was an opaque layer of 120 nm of Au and the top electrode was a semi-transparent layer of 10 nm of Ag. As electron transporting layer (ETL) we used a layer of ZnO and as hole transporting layer (HTL) a layer of MoO_3. On top of the Ag electrode we deposited a two-layer ARC made of MoO_3 and LiF. For the semi-transparent devices we used the exact same architecture except that the Au electrode was thinned down to 13 nm. We used the same active material and blocking layers as in the opaque cell, while we used two different configurations for the external light harvesting structure. As seen in Figure 1, for STC1 we incorporated in between the Au electrode and the substrate a six-layer 1-dimensional MLD made alternating TiO_2 and

SiO_2. This structure was designed numerically to maximize the current while keeping the overall visible transparency of the solar cell above 20%. In such design we used an inverse integration procedure[1] based on the transfer matrix formalism[1, 24] to determine numerically the relative thicknesses of all layers in the MLD and ARC. As in Ref. [1] the optimal cell structure was obtained by considering the contribution from all layers in a single numerical inverse integration. As seen in Figure 1, STC2 did not incorporate any MLD. Both, STC1 and STC2 are ITO free cells incorporating the same ARC on top of the Ag electrode we used for the opaque one. The metallic behavior of both electrodes, ensured a higher degree of light trapping for STC1 and STC2, while, as we shall see below, light trapping in STC2 was rather limited.

As shown in **Figure 2**, the transparency of STC1 relative to STC2 increased between 430 nm and 510 nm and in the blue part of the spectrum while experiencing a slight reduction in the rest of the visible spectrum. STC1 exhibited a considerable reduction in transparency beyond 600 nm up to 770 nm. The overall visible transparency was similar when comparing STC1 with STC2, however, as seen in Figure 2, the combination of the MLD and ARC to trap light in the near IR slightly enhanced transparency in the blue for STC1.

To evaluate the PV performance of the two semi-transparent devices we performed J-V measurements under 100 mW/cm^2 illumination from an AM1.5G solar simulator. The corresponding J-V curves and PV parameters were compared with the corresponding measurements from the opaque cell. As may be seen in **Figure 3** and **Table 1**, the J_{sc} from the STC1 device is close to double the one from the STC2. Remarkably, as seen in Figure 3, the J_{sc} for STC1 is equivalent to 96.4% the one for the opaque cell. On the contrary, the lack of an effective light trapping structure for STC2 leads to a J_{sc} which is, in that latter case, only 53%

the one for the opaque cell. When comparing the other PV parameters, summarized in Table 1, we observe a minor decrease in the V_{oc} in the amount of 2% from the opaque solar cell to both transparent ones, STC1 and STC2. Similarly, a minor decrease is observed for the FF from the opaque solar cell in the amount of 2.5% for STC2 and 5.7% for STC1. Such minor reduction observed in the FF can be, to a large extent, attributed to an increase in the series resistance clearly visible in Figure 3 when thinning down the gold electrode. The deposition of such electrode on top of the MLD has also a minor influence on the electrical characteristics of the solar cell provided that the observed decrease in FF is slightly larger for STC1 than for STC2. In fact, the thin gold electrode of STC2 was deposited on a polished glass, while for STC1 was deposited on top of the MLD comprising six sputtered dielectric thin films. In any case, since the FF and V_{oc} were affected only marginally by the MLD (cf. Table 1), the PCE of STC1 was 1.8 times larger than the one from STC2.

In correspondence to the short circuit currents, in the experimentally measured EQEs, shown in **Figure 4a,** we observe that the STC1 and Opaque devices behave similarly while the STC2 exhibits a significantly reduced EQE. Indeed, in the entire absorption wavelength range there is a remarkable match between the STC1 and Opaque EQEs. In other words, in the semi-transparent configuration considered for the STC1 cell the light harvesting capacity of the original cell is maintained for the full spectrum of interest. The main features observed in the EQEs of the fabricated devices were well predicted using the model developed to design the MLD and the ARC, which we used, here, to determine numerical EQEs shown in Figure 4b.

The similarity between the STC1 and Opaque EQEs suggests a more effective light trapping capacity at the wavelengths of interest when the active layer is embedded in between to metal electrodes forming an optical cavity. Using this same model to compute the EQEs we

determined the electric field intensity distribution at any given wavelength or position within the active layer. Such maps are shown in Figure 5 for the STC1 and Opaque configurations and an additional opaque configuration where the semi-transparent electrode formed by a thin metal combined with a MoO_3 layer is replaced by the standard ITO layer.

To properly visualize differences in the light trapping character in between the several configurations computed, the extinction coefficient was taken to be zero everywhere except in the metallic layers. When comparing Figures 5a and 5b, one sees that a similar light trapping capacity for the STC1 and Opaque cells in the 500 nm to 750 nm wavelength range. This trapping appears to be in both cases almost wavelength independent for a large part of the wavelength range of interest. On the contrary, the ITO-Opaque configuration, whose field distribution is shown in Figure 5c, exhibits a clear interference pattern with several regions where the trapping capacity is clearly diminished.

We conclude that when the OPV architecture includes two thin metallic electrodes, one of them being assisted with an MLD to enhance reflectivity for the case of semi-transparent cells, one may obtain a broadband photon trapping capacity sufficient to match the performance of semi-transparent cells to opaque ones. We demonstrated that it is the combined effect of an MLD and a thin metal layer that prevents, to a large extent, the loss in photon harvesting capacity exhibited by the majority of semi-transparent cells. Indeed, the J_{sc} for a cell device incorporating such cavity configuration, which exhibited a 21% visible transparency, amounted to 96.4% the J_{sc} of the corresponding opaque cell. As shown in Figure S1 from the supporting information file, it is possible to optimize the optical cavity opaque cell configuration to obtain a J_{sc} equivalent to the one obtained from a standard PTB7:$PC_{71}BM$ cell where the light entering electrode is an ITO layer. In that event, as reported in Table S2,

the use of a multilayer would lead to a semi-transparent cell with a J_{sc} equivalent to 87% the one from the opaque counterpart cell and 92% the one form the standard cell. This sets the upper limit efficiency for semi-transparent cells using PTB7 as the donor polymer to 7%. However, as seen in Table S1, fabrication of such optimized cavity configuration cell would require the use of a 5 nm ZnO buffer layer which can not be obtained under the standard sol-gel procedure commonly used.

In the fabricated cells we observed a small reduction in the other two PV parameters when thinning down the Au electrode led to a final PCE for the semi-transparent cell assisted with near IR light trapping of 90% the one for the opaque cell. The 21% visible transparency we demonstrated here may find applications in PV building integration where 20% average visible transparencies are acceptable. In the event that such MLD configuration would be applied to polymers with a red shifted absorption relative to the PTB7, higher degrees of transparencies in the visible would be achievable. This would extend the areas for application of such PV technology to power up electronic devices where higher visible transparencies may be required.

Experimental

Multilayer fabrication: The fabricated devices were grown on soda-lime glass substrates. The SiO_2 and TiO_2 thin films of the MLD were grown using reactive magnetron sputtering in high vacuum[25-27]. Argon was used as sputter gas and oxygen as reactive gas. The SiO_2 films exhibited a refractive index about 1.49 at 550 nm, while the TiO_2 thin films exhibited a refractive index about 2.45 at 550 nm. The MLD was deposited close to normal incident to prevent any optical problem related to refractive index decrease due to an increment in the

porosity of the film. As indicated below, on top of the MLD we deposited, by thermal evaporation, a thin layer of Au as electrode before proceeding with the PV device fabrication.

Device fabrication: A ZnO film was deposited by spin-coating on top of the gold electrode and thermally annealed on a hotplate in air (200 °C during 30 min) resulting in a 30 nm thick layer. The PTB7:$PC_{71}BM$ (1:1.5 wt in CB) layer was deposited by spin-coating and treated by solvent annealing during 5 min and by vacuum annealing during 30 min to obtain a 90 nm layer. Finally, a 10 nm MoO_3 was thermally evaporated and to finish the devices a Ag thin electrode was deposited.

ARC and metal electrodes fabrication: Both the transparent and the opaque gold electrodes were thermally evaporated in a high vacuum system (Mini SPECTROS™, Kurt J. Lesker Company). The speed of deposition for gold was 3 Å s^{-1} to obtain a final thickness of 13 nm for the semi-transparent cells and 120 nm for the opaque one. To complete the cell we thermally evaporated a transparent thin Ag electrode on top of the MoO_3 previously deposited. The deposition rate for Ag was 5.5 Å s^{-1} while the sample was placed on a cooled holder in order to decrease Ag surface diffusion and therefore prevent 3D island growth by altering the standard nucleation process[28]. The Ag electrode was deposited using masks made with laser beam cutting technology which yielded well-defined cell areas. Finally, on all cells, we deposited a two layer ARC comprising a layer of MoO_3 (n=2.17 at 550 nm) and a layer of LiF (n=1.24 at 550nm). The deposition rate for such materials were 1 Å s^{-1}. Pellets/stones were used as material for evaporation. The residual vacuum pressure was below 10^{-6} torr in order to prevent any contamination. The ARC was deposited close to normal incident. The thickness for all evaporated layers was monitored using a crystal oscillator during deposition and later

verified from the transmission curves adjusted using the calculated electromagnetic field transmission.

Measurement systems: Electrical characterization (J-V measurements) was done employing an ABET technologies Sun 3000 solar simulator under AM1.5G illumination conditions and a Keithley 2420 source meter. The external quantum efficiency was measured with a solar cell spectral response measurement system from PC measurements, inc. model QEX10. The integration of the EQE spectra under the AM1.5G solar spectrum yielded J_{sc} values that were consistent with the ones obtained from the J-V measurements (reported in Table 1).

Acknowledgements
This work was supported by the European Commission through the Erasmus Mundus Joint Doctorate Programme Europhotonics (Grant No.159224-1-2009-1-FR-ERA MUNDUS-EMJD) and by the Ministerio de Economía y Competitividad with the grants MAT2011-28665, IPT-120000-2010-29 and IPT-2012-0986-120000.

Received: ((will be filled in by the editorial staff))
Revised: ((will be filled in by the editorial staff))
Published online: ((will be filled in by the editorial staff))

_[1] Betancur R., Romero-Gomez P., Martinez-Otero A., Elias X., Maymó M. & Martorell J., *Nature Photon.* **2013**, *7*, 995-1000.

_[2] C. Chen, L. Dou, J., W. Chang, G. Li and Y. Yang, *Energy Environ. Sci.* **2013**, *6*, 2714

_[3] C.-C. Chueh, S.-C. Chien, H.-L. Yip, J. F. Salinas, C.-Z. Li, K.-S. Chen, F.-C. Chen, W.-C. Chen, A. K.-Y. Jen, *Adv. Energy Mater.* **2013**, *3*, 4, 417–423.

_[4] R. F. Bailey-Salzman, B. P. Rand and S. R. Forrest, *Appl. Phys. Lett.* **2006**, *88*, 233502.

_[5] G.-M. Ng, E. L. Kietzke, T. Kietzke, L.-W. Tan, P.-K. Liew and F. Zhu, *Appl. Phys. Lett.* **2007**, *90*, 103505.

_[6] F.-C. Chen, J.-L. Wu, K.-H. Hsieh, W.-C. Chen and S.-W. Lee, *Org. Electron.* **2008**, *9*, 1132–1135.

_[7] A. Colsmann, A. Puetz, A. Bauer, J. Hanisch, E. Ahlswede, U. Lemmer, *Adv.Energy Mater.* **2011**, *1*, 599–603.

_[8] F. Guo, X. Zhu, K. Forberich, J. Krantz, T. Stubhan, M. Salinas, M. Halik, S. Spallek, B. Butz, E. Spiecker, T. Ameri, N. Li, P. Kubis, D.M. Guldi, G. J. Matt and C. J. Brabec, *Adv. Energy Mater.* **2013**, *3*, 8, 1062–1067.

_[9] Z. Tang, Z. George, Z. Ma, J. Bergqvist, K. Tvingstedt, K. Vandewal, E. Wang, L. M. Andersson, M. R. Andersson, F. Zhang, O. Inganäs, *Adv. Energy Mater.* **2012**, *2*, 12, 1467–1476.

_[10] J. Krantz, T. Stubhan, M. Richter, S. Spallek, I. Litzov, G. J. Matt , E. Spiecker and C. J. Brabec, *Adv. Funct. Mater.* **2013**, *23*, 13, 1711–1717.

_[11] C. Tao, G. Xie, C. Liu, X. Zhang, W. Dong, F. Meng, X. Kong, L. Shen, S. Ruan and W. Chen, *Appl. Phys. Lett.* **2009**, *95*, 053303.

_[12] L. Shen, Y. Xu, F. Meng, F. Li, S. Ruan, W. Chen, *Org. Electron.* **2011**, *12*, 1223–1226.

_[13] C. Tao, G. Xie, F. Meng, S. Ruan and W. Chen, *J. Phys. Che. C* **2011**, *115*, 12611–12615.

_[14] T. Winkler, H. Schmidta, H. Flüggea, F. Nikolayzika, I. Baumanna, S. Schmalea, T. Weimannc, P. Hinzec, H.-H. Johannesa, T. Rabea, S. Hamwia, T. Riedlb, W. Kowalskya, *Org. Electron.* **2011**, *12*, 1612–1618.

_[15] Z. Liu , J. Li , Z.-H. Sun , G. Tai , S.-P. Lau and F. Yan, *ACS nano* **2012**, *6*, 810–818.

_[16] J. Huang, G. Li, and Y. Yang, *Adv. Mater.* **2008**, *20*, 415–419.

_[17] J.-Y. Lee, S. T. Connor, Y. Cui and P. Peumans, *Nano Lett.* **2010**, *10*, 1276–1279.

_[18] R. R. Lunt and V. Bulovic, *Appl. Phys. Lett.* **2011**, *98*, 113305.

_[19] N. P. Sergeant, A. Hadipour, B. Niesen, D. Cheyns, P. Heremans, P. Peumans and B. P. Rand, *Adv. Mater.* **2012**, *24*, 728-732.

_[20] H. Jin , C. Tao, M. Velusamy, M. Aljada, Y. Zhang, M. Hambsch, P. L. Burn and P. Meredith, *Adv. Mater.* **2012**, *24*, 2572–2577.

_[21] D.S. Ghosh, R. Betancur, T.L. Chen, V. Pruneri and J. Martorell, *Sol. Energy Mat. Sol. Cells* **2011**, *95*, 4, 1228-1231.

_[22] N. Formica, D. S. Ghosh, T. L. Chen, C. Eickhoff, I. Bruder, V. Pruneri, *Sol. Energy Mat. Sol. Cells* **2012**, *107*, 63-68.

_[23] F.-C. Chen, J.-L. Wu, K.-H. Hsieh, W.-C. Chen, and S.-W. Lee, *Org. Electron.* **2008**, *9*, 1132–1135.

_[24] R. Betancur, A. Martínez-Otero, X. Elias, P. Romero-Gómez, S. Colodrero, Hernán Miguez, and J. Martorell, *Sol. Energy Mat. Sol. Cells* **2012**, *104*, 87–91.

_[25] J. M. García-Martín, R. Alvarez, P. Romero-Gómez, A. Cebollada, and A. Palmero, *Appl. Phys. Lett.* **2010**, *97*, 173103.

_[26] R. Alvarez, P. Romero-Gomez, J. Gil-Rostra, J. Cotrino, F. Yubero, *J. Appl. Phys.* **2010**, *108*, 064316.

_[27] R. Alvarez, P. Romero-Gomez, J. Gil-Rostra, J. Cotrino, F. Yubero, A. R. Gonzalez-Elipe and A. Palmero, *Phys. Status Solidi* **2013**, *A210*, 4, 796–801.

_[28] N. P. Sergeant, A. Hadipour, B. Niesen, D. Cheyns, P. Heremans, P. Peumans and B.P. Rand, *Adv. Mater.* **2012**, *24*, 728-732.

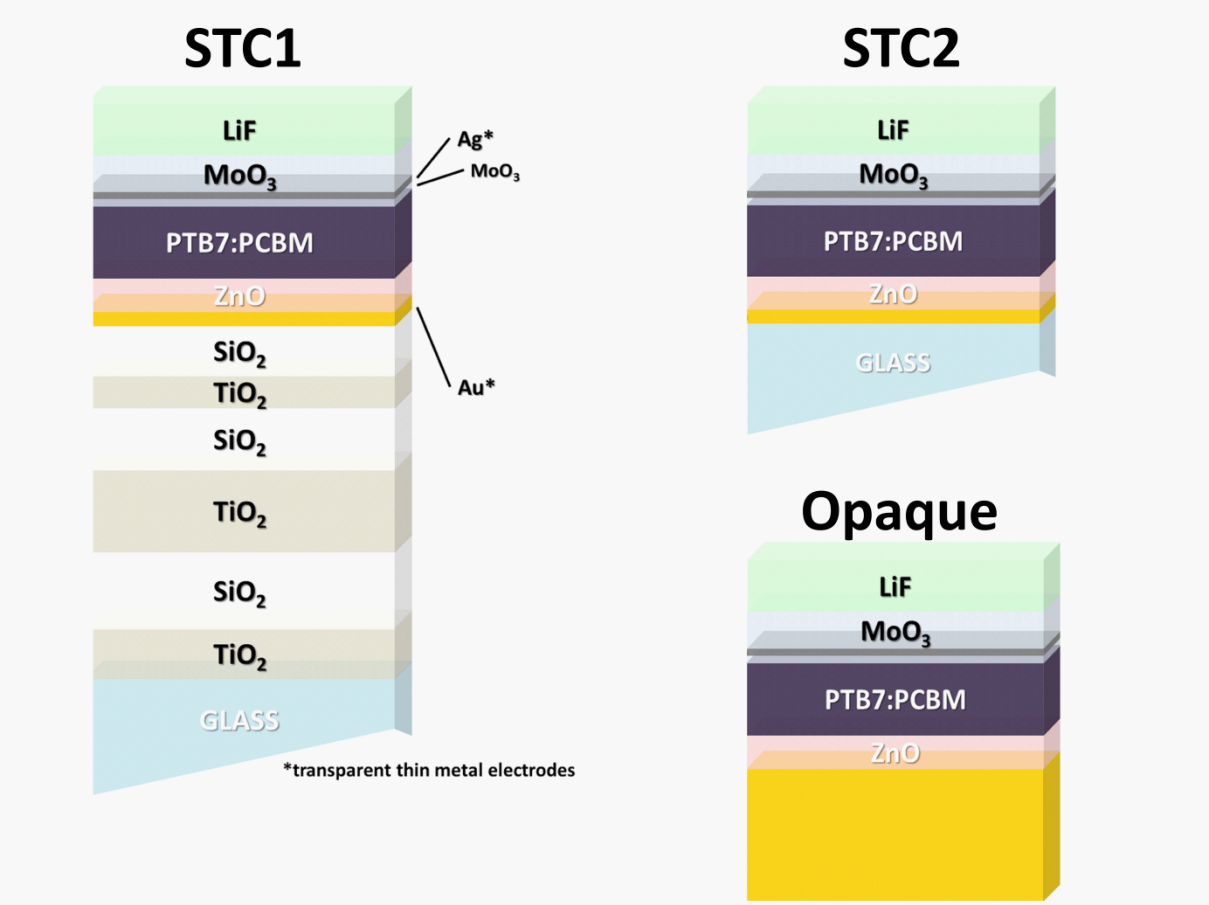

Figure 1. Schematic illustration of the semi-transparent device cell architecture incorporating the MLD between the glass and the Au thin metal electrode and ARC above the Ag thin metal electrode. Near IR light is partially confined in the active layer (PTB7:PCBM) while the visible transparency for the device is kept above 20 %.

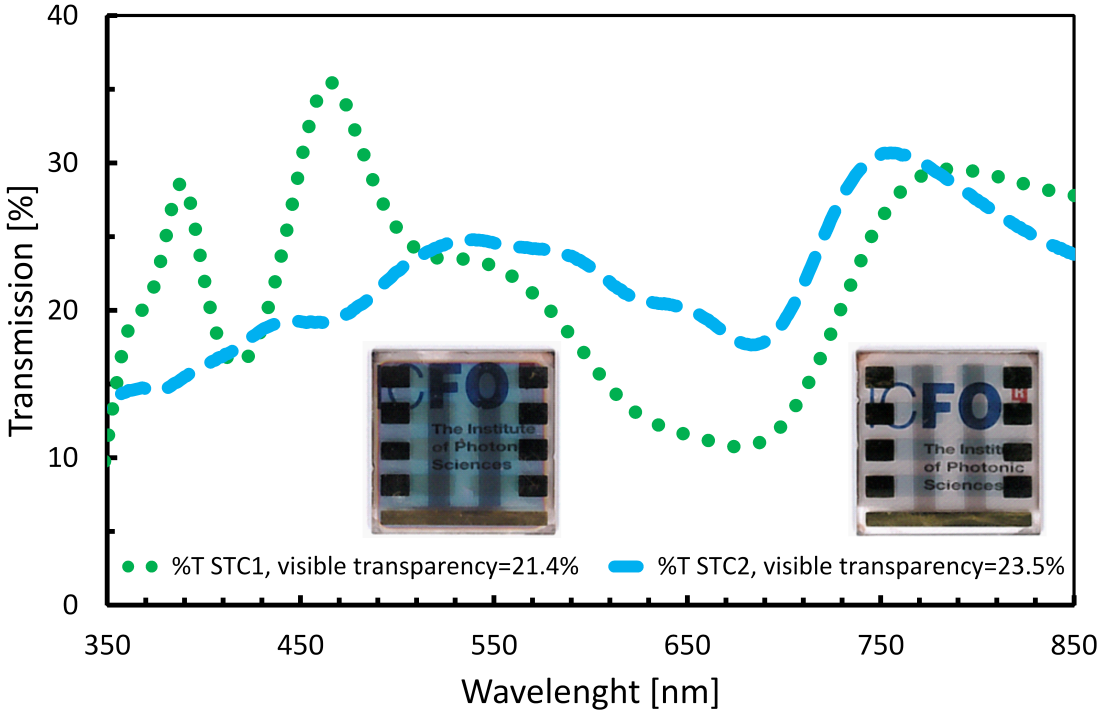

Figure 2. Light transmission for STC1 (dotted line) and for STC2 (dashed grey line). Inset: Picture of STC1 (top image) and STC2 (bottom image).

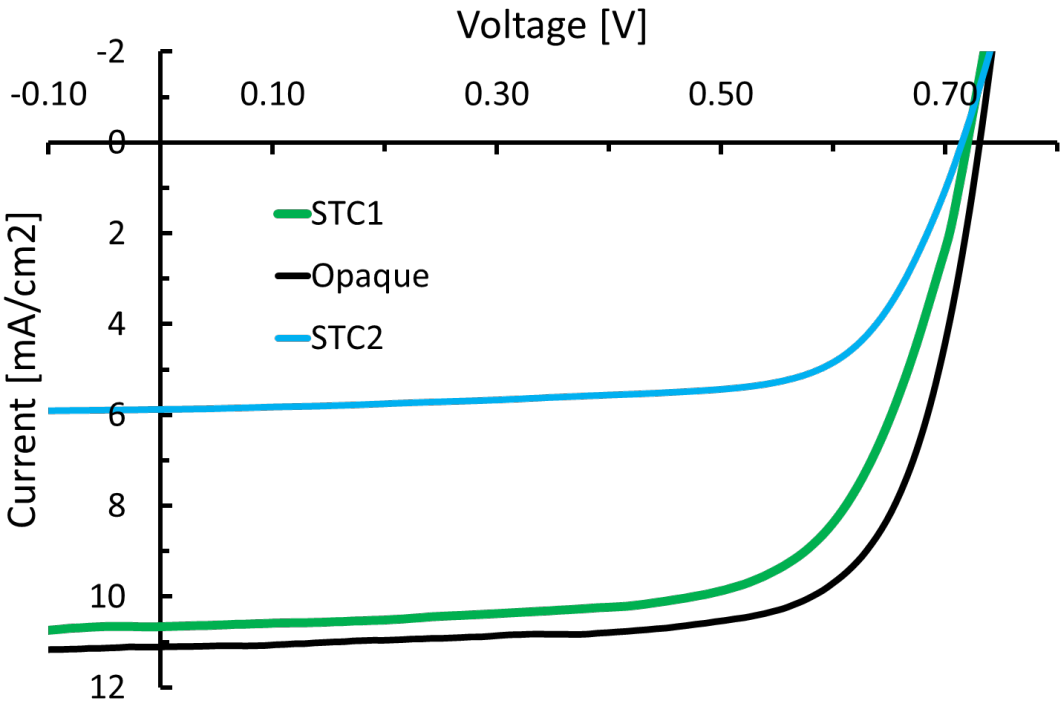

Figure 3. Measured J-V curves for the semi-transparent device (STC1) shown in Figure 1 (solid green) for the STC2 (solid cyan), and for the opaque solar cell (solid black).

a)

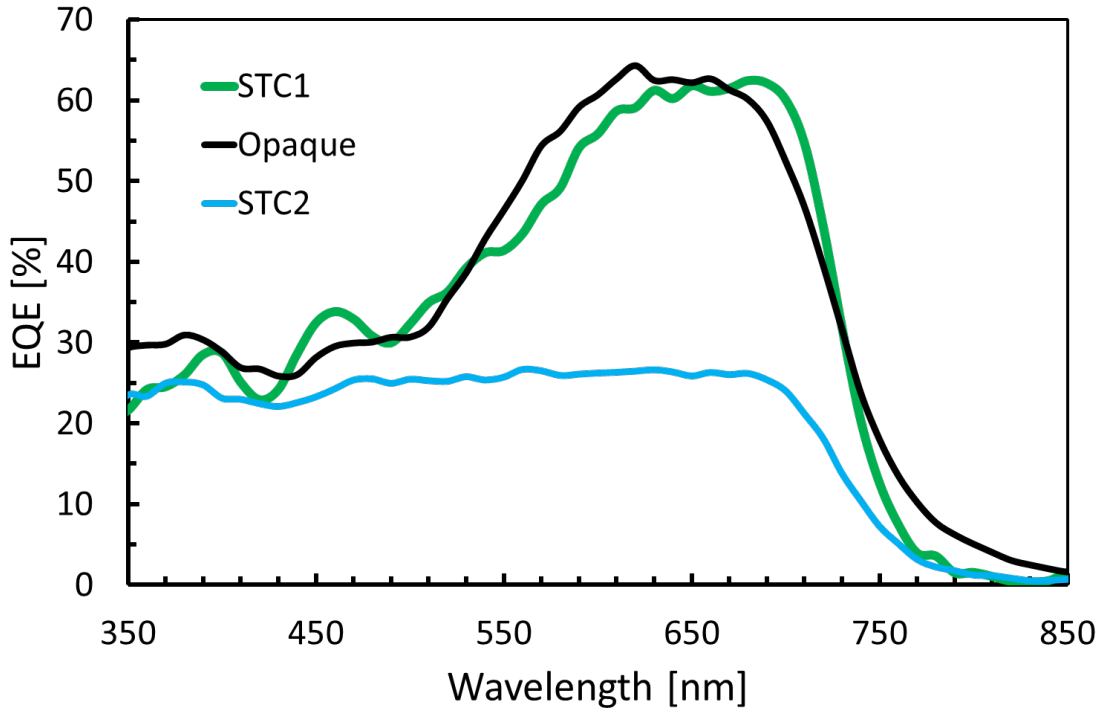

b)

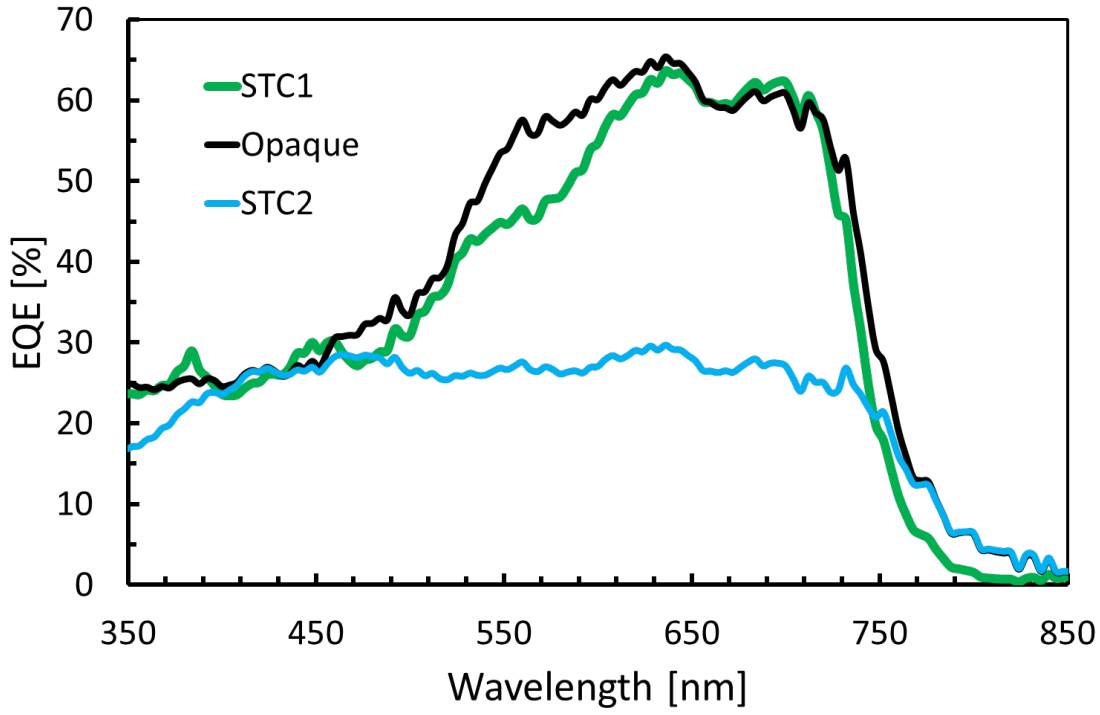

Figure 4. Experimentally measured (a) and Simulated (b) external quantum efficiencies for the semi-transparent device showed in the Figure 1 incorporating the MLD (in green) a semi-transparent solar cell without light trapping (in cyan) and the opaque solar cell (in black). The small oscillations in the numerically computed EQEs partially originate from noise in the experimental determination of the index of refraction of the blend.

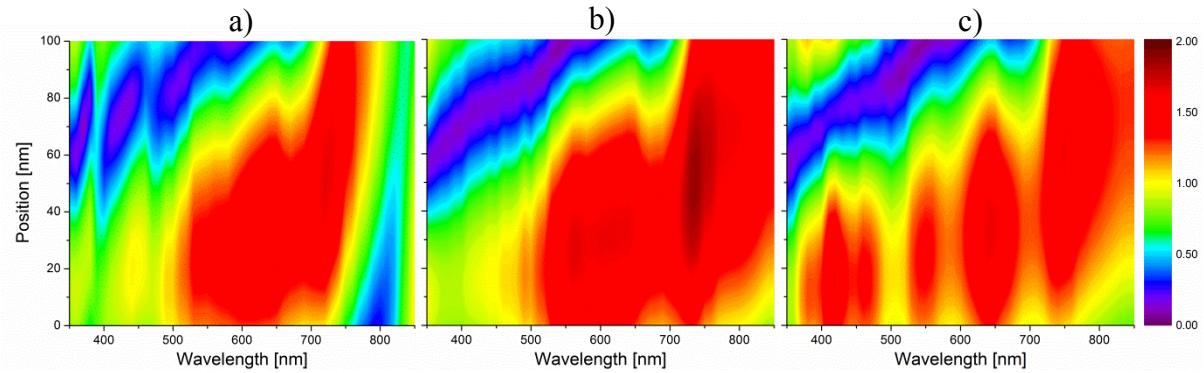

Figure 5. Numerically computed field intensity maps for the (b) STC1, (c) Opaque, and (d) ITO Opaque configurations. To properly visualize differences in light trapping character, in all these numerical computations the extinction coefficient was taken to be zero everywhere except in the metallic layers. In the vertical axis zero corresponds to the active layer-MoO_3 interface, i.e. the one closest to the thin Ag light entering electrode. All fields are normalized to the input field intensity.

Table 1. Solar cell J-V characteristics.

Solar cell device	J_{sc} [mA cm^{-2}]	J_{sc}/J_{sc}^{MAX} [ratio]	Voc [V]	FF [%]	Eff [%]	Visible Transparency [%]
STC1	10.7	0.964	0.728	67.9	5.3	21.4
Opaque	11.1	1	0.739	72.0	5.9	-
STC2	5.9	0.532	0.723	70.2	3.0	23.5